Collett, M. A., Gamlath, C., & Cryan, M. (2017). An optically tunable cavity-backed slot antenna. *IEEE Transactions on Antennas and Propagation*. https://doi.org/10.1109/TAP.2017.2755726

An Optically Tunable Cavity-Backed Slot Antenna

M A Collett, C D Gamlath and M J Cryan

***Abstract*— There is a growing pressure on antenna designers to provide ever increasing operating bandwidth, efficiency and flexibility. Emerging communications standards are requiring operation over wide frequency ranges, often with multiple, separated bands of operation. This paper proposes and demonstrates an optically tunable cavity backed slot antenna. Through the incorporation of four silicon bridging pieces and a fiber coupled laser, the operating frequency can be tuned between 4.2 GHz and 6 GHz. Antenna efficiency has been measured and ranges between 36% and 62% depending upon the combination of frequency and tuning state, with the gain taking values between 4.3 dBi and 6.9 dBi. An effective fabrication process for the incorporation of silicon into the antenna has been described, as well as methods for effectively simulating the optically generated conductivity. Simulations and measurements show good agreement, and several proposed improvements are proposed for this novel and flexible tuning technology.**

***Index Terms*— Tunable Antenna, Optical Tuning, Simulation, Measurement, Multi Frequency.**

I. Introduction

Wireless communications systems are becoming increasingly complex. Many new communications protocols are no longer relying on single contiguous blocks of spectrum, but are designed to simultaneously utilize several bands which can be far apart[1]. For short range, very high data rate applications, there is much ongoing research into high frequency communications systems, particularly around 60 GHz [2]. Such high frequency systems introduce new challenges with high path loss necessitating high gain and steerable antennas. This tunability and steering needs to be implemented without introducing excessive distortion into the system. Conventional tuning approaching rely on varactor or PIN diodes [3-5] or more recently MicroElectroMechanical Systems (MEMS) switches[6-8]. These approaches have a number of drawbacks, the main one being that they require bias networks to control the tunable devices. In the case of simple antennas at low frequencies this is achievable, however with large antenna arrays and at higher frequencies such bias networks can significantly affect the system performance. The other important issue is that of non-linearity, in the case of diode tuning, intermodulation distortion can be a major effect, especially on the transmit side where powers are high[4,5]. MEMS based system are more linear than diodes, but there remain a number of issues to be solved before their widespread adoption takes place, in particular around reliability and "hot" switching [6,7].

In this paper we demonstrate a novel tuning methodology based upon optically generated conductivity in a semiconductor which overcomes many of the issues outlined above. This approach has been researched for a number of years [9,10] and relies on the generation of an electron-hole plasma at the surface of a semiconductor. This occurs when the semiconductor is illuminated with light with energy greater than the semiconductor band gap. Thus the main advantage is that there is no physical connection between the tuning mechanism (the light source) and the microwave circuits. This removes the requirement for bias circuits and allows for very large arrays to be illuminated with many light sources simultaneously. A further important advantage is that the electron-hole plasma has no inherent PN junction and thus has no diode based non-linearity. Initial assessments of the linearity of this approach have been carried out [11] and these show linearity similar to MEMS based devices. There is a significant disadvantage to optical tuning, the requirement for a light source, which can require a number of watts of electrical power to operate. However, very rapid progress in laser and LED design has occurred over the past 20 years and now high power laser [12] and LED arrays[13] are becoming available which allow optical tuning technology to be implemented. This is most likely to be in applications where the extra DC power for the light source is not critical to the overall system design such as in radars or mobile phone base stations, but where high linearity and reliability is important.

Optically controlled antennas have been studied previously and [14] shows results for a planar microstrip dipole antenna. This paper shows results for a cavity backed slot antenna design that could be useful in higher power transmit antennas where the majority of the radiation should be in the forward direction. High efficiency operation is obtained along with wide band tuning and pattern switching effects which show potential for application in future communication and radar systems.

The paper is structured as follows : Section II shows the optically induced conductivity profiles that are used in 3D full wave modelling. Section III describes the fabrication of the antennas. Section IV shows the simulated performance using CST Microwave Studio. Section V shows the measured results and Section VI draws conclusions

This work is supported by the Engineering and Physical Sciences Research Council (EP/I028153/1) and the University of Bristol. Submitted for consideration in August 2016

II. Optical Interactions with Silicon

There are a number of processes that occur when a semiconductor is illuminated with light including electron-hole pair generation, recombination and carrier diffusion. These are well understood and we have used this physics to develop a 3D electromagnetic model for the microwave behavior of these plasmas which is outlined in [15]. Using this approach the conductivity profile within intrinsic silicon under differing illumination powers is shown in (b)

Figure 1**(a). The parameters used here are wavelength=980nm, absorption coefficient, α=100cm^{-1} [16] (equivalent to absorption depth of 100μm), bulk carrier lifetime, τ_{Bulk}=10μs [15], surface recombination velocity S=20 cms^{-1}[15] and diffusion length, L_n=120μm[15]. It can be seen that the illumination causes a conductivity maximum close to the silicon surface, and the generated charge carriers diffuse exponentially away from the surface. The drop in conductivity at the surface is related to the surface recombination velocity and represents the effects of surface states [15].** (b)

Figure 1 also shows how the modelled conductivity profile is converted into nested blocks of differing material properties, which will be subsequently incorporated into the simulation model.

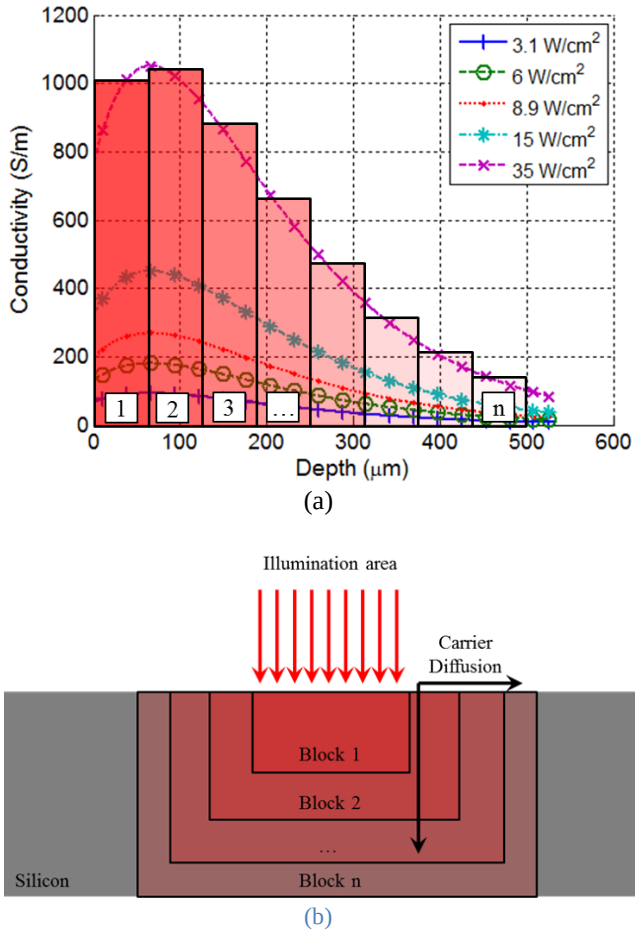

Figure 1 – (a) Depth conductivity profile in silicon resulting from several different illumination powers showing conductivity blocks used in modelling and (b) 2D Block structure including effects of lateral carrier diffusion

III. Antenna Design and Fabrication

In order to demonstrate this tuning methodology, whilst maintaining practical parameters of device size, operating frequency and measureability, it was decided to fabricate a simple slot antenna operating close to 5 GHz. Shown in Figure 2, the design consists of a 33.6 mm × 2 mm slot machined into a 0.7 mm thick brass ground plane, the slot was backed with a 54 mm × 54 mm × 17 mm cavity, with the 17 mm depth chosen to be close to one quarter of the operating wavelength, giving constructive forward addition between the direct radiation from the slot, and that reflected from the inside back wall of the cavity. The cavity acts to increase the directivity of the antenna, and also aid measurement. The antenna can be easily mounted on a rotation stage for pattern measurement, with the main beam facing away from the mounting equipment (a slot without cavity would radiate equally in both directions, causing perturbations and interactions with any mounting equipment or stand). Tunability is afforded by the incorporation of four bridging pieces, spaced at 2 mm intervals from one end of the slot. Each bridging piece consists of a 1.3 mm × 10 mm × 0.38 mm piece of un-doped silicon wafer. On to the cleaned,

etched wafer is sputter coated 500 nm of gold (with a 10 nm titanium adhesion layer). Photolithography is used to create a 0.3 mm gap in the gold and titanium, giving a very precise slot in the metallization. The metallized parts of the silicon were then bonded to the brass ground plane using conductive silver epoxy adhesive. Small silicon pieces were chosen as opposed to filling the whole slot, in order to reduce dielectric losses of the antenna (where high fields in the dielectric material are likely to cause inefficiencies). The photolithography with preceding cleaning and etching provides a good electrical bond between the metallization and silicon, reducing the potential Ohmic losses caused by impurities or the naturally occurring silicon dioxide layer which would otherwise be present on the silicon. The size and spacing of the silicon pieces were chosen following a trade-off between antenna efficiency and tuning range, but many options would be possible depending upon the desired antenna behavior. A preliminary simulation parameter sweep determined the best position of the feed, consisting of a coaxial cable with the outer ground sheath bonded to one side of the slot in the brass plane, with the central conductor bonded to the opposite side. The positioning was intended to give a good match across all tuning states, and was found to be 6 mm from the slot end.

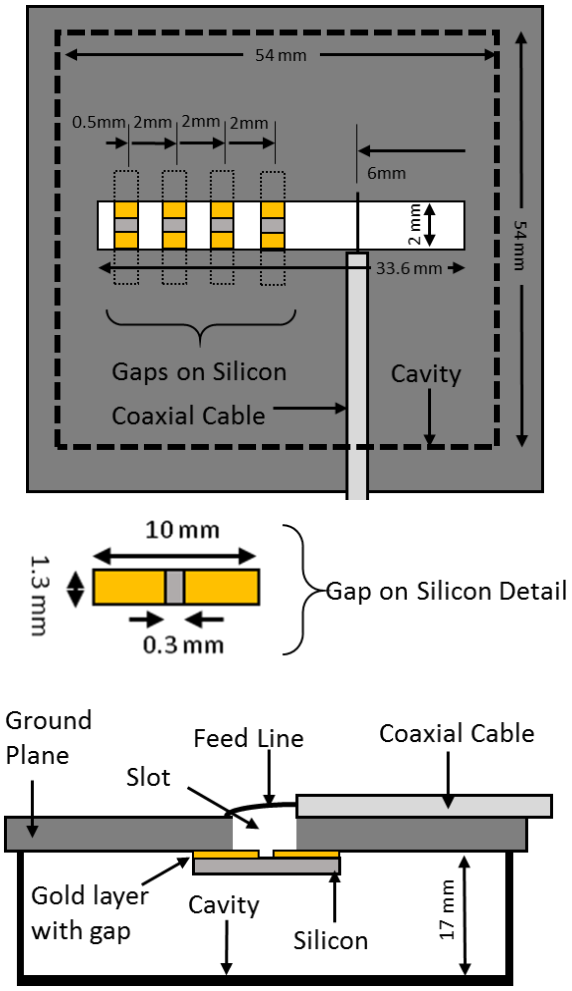

Figure 2 - Schematic showing antenna design (top), detail of 500nm gold, with gap on silicon piece (middle), and vertical elevation (bottom).

Illumination is provided by a 980 nm fiber coupled laser diode, with a maximum total optical power output of 2 W. For this set of measurements, the total output power was maintained at 1 W and illuminates the desired silicon bridging piece directly, achieving an intensity of 35 Wcm^{-2}. For the purposes of this work, the optical efficiency was not investigated, with the main focus being on the tunability and antenna operating parameters. Practical designs could employ integrated optical sources, or potentially an addressable array coupled with a micro lens array or light pipe in order to achieve the same level of tunability with significantly reduced optical power. The fabricated antenna and the positions and mounting of the fiber illumination are shown in Figure 3. A laser cut acrylic fiber holder was designed and constructed to allow accurate and secure positioning of the fiber at the desired locations. Additionally, the gold layer provides a natural optical mask ensuring that the illumination only falls on the desired silicon position.

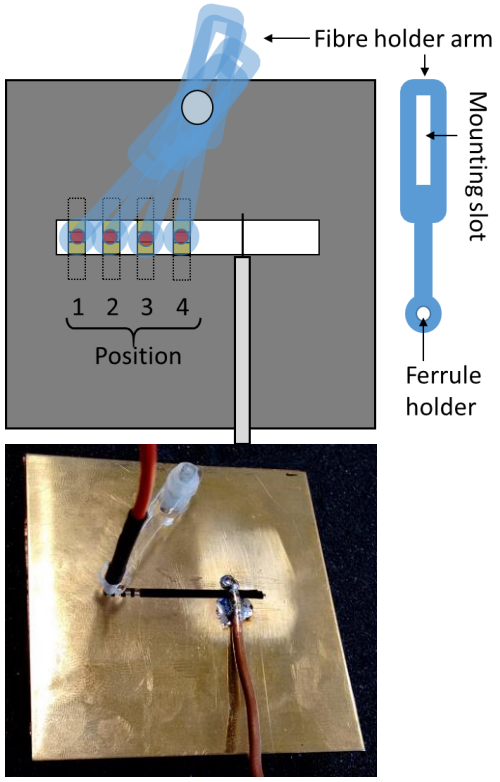

Figure 3 - Schematic of cavity backed slot antenna with four photoconductive slot pieces, showing fiber illumination positions (top), photograph (bottom).

IV. Simulated Behavior

Several simulations were carried out to predict the antenna behavior under differing illumination conditions. The geometry and material properties were recreated in CST Microwave Studio [17], with the simulated frequency range set to 0 GHz to 20 GHz, with farfield monitors set up at 500 MHz intervals between 2 GHz and 11 GHz to allow efficiency predictions over that range. Following the methodology in (b)

Figure 1, the optically generated conductivity was recreated by incorporating several nested blocks of appropriate electrical properties (conductivity and permittivity), following the curve for 35 Wcm^{-2} giving a surface conductivity of 1000 Sm^{-1}. The resultant predicted return loss for the five illumination states (each of the positions illuminated in turn, as well as the unilluminated case) are shown in Figure 4. This shows the clear tuning effect of the illumination as it is applied at each of the positions. As intended the match improves from -12 dB at 4.25 GHz to around -20 dB at 4.5 GHz (the trend implies that the best match may occur around 4.8 GHz, but there are no tuning states at this frequency). Additionally the total tuned range 10 dB bandwidth is 1.85 GHz or 37% albeit with some small gaps within that band. Further design refinements could ensure that each of the tuned states were sufficiently close to offer a continuous sub -10 dB match over the whole tuned range.

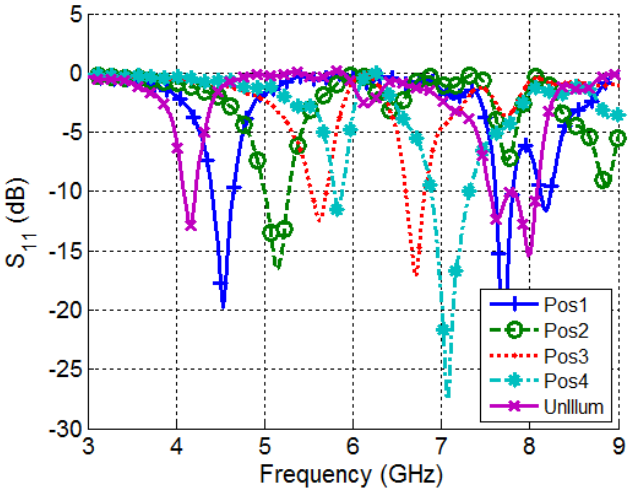

Figure 4 - Simulated return loss for cavity backed slot antenna for each of tuning states.

In order to determine whether the return loss tuning seen in Figure 4 gives rise to a corresponding radiative tuning effect, the predicted antenna efficiency was also simulated at each antenna state. This is calculated by first simulating the full 3D radiation pattern and then integrating the energy at a given frequency incident upon the bounding walls of the simulated volume. This is then compared to the port input energy at that frequency. The resultant predicted efficiency behaviors are shown in Figure 5.

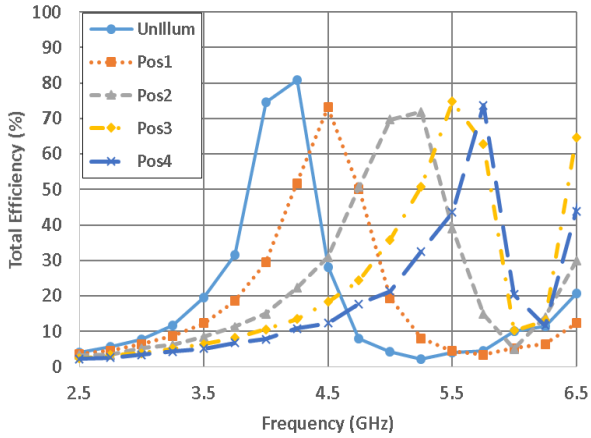

Figure 5 - Simulated total efficiencies of the cavity backed slot antenna for each of the illumination positions (top) and zoomed selection (bottom).

The predicted efficiency profile can be seen to largely follow the return loss resonance ranges, with the fundamental resonance at 4.25 GHz moving up to 5.8 GHz. The entirety of the tuned range from 3.9 GHz up to 5.9 GHz maintains an efficiency of 50% or above, with each of the peaks around 75% efficient. There is a relatively strong null in radiation around 6.3 GHz, with none of the tuned states giving an efficiency greater than 11% at this frequency. This may be due to some mismatch resonance within the feed structure preventing energy getting to the slot, or potentially the cavity itself having a destructive resonance.

V. Measured Behavior

The fabricated antenna was first characterized using a Vector Network Analyzer (VNA), with the return loss measured for each of the five tuning states. The measured results are shown in Figure .

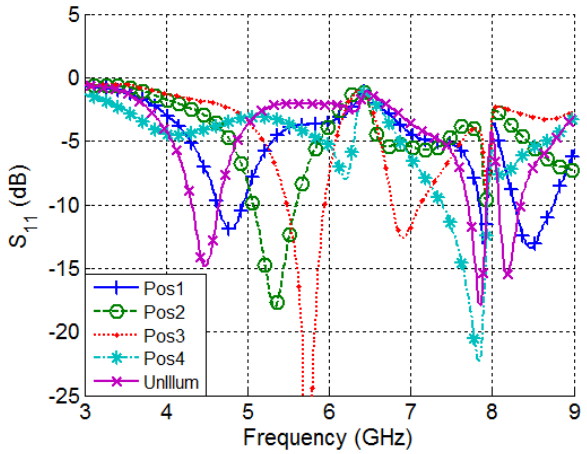

Figure 6 - Measured return loss of illuminated cavity backed slot antenna with photoconductive pieces for five tuning states.

As the illumination is applied, and moved through positions further from the edge of the slot, it can be seen that there is a clear tuning effect, with the main resonance moving from 4.5 GHz up to 5.75 GHz. The total tuned range 10dB bandwidth is 1.75 GHz or 35% of the center of the tuning range. Interestingly, with illumination at Position 4, closest to the center of the slot, the antenna shows no clear resonance close to this range. This is likely to be caused by the limitations of the feed matching; as the effective slot length and resonant frequency change, so does the position of the 50 Ohm point. Eventually the feed will be poorly matched. Additionally, there is a strong mismatch at 6.4 GHz, which does not vary with illumination. This strong mismatch may be caused by the cavity resonance. Predictions for an unslotted and unloaded cavity show that 17 mm deep gives an in phase constructive match at 4.6 GHz, but will have a reflected component 90° out of phase at around 5.7 GHz. For the slotted slightly loaded case, these frequencies may be shifted, giving the strong narrow mismatch at 6.4 GHz. In future we will investigate other feeding mechanisms such as proximity feeding which can be more broadband in nature.

Comparing the measured return loss result in Figure 6, with the simulated return loss result in Figure 4, it can be seen that there is good agreement with the general tuning trend for all of the states, except for Position 4, which in the simulated case shows a reasonable -11 dB resonance at 5.8 GHz, compared to a -7 dB resonance at 6.2 GHz. For each of the other tuning states there is good agreement, with any small differences in frequency or match resulting from fabrication tolerances.

In order to verify the radiative nature of the tuning, as predicted by simulations in Figure 5, the efficiency measurement technique described in [18] was employed. This technique involves measuring the full 3D pattern from the antenna under test at the chosen frequency. A highly efficient reference monopole antenna at the chosen frequency is also measured. The total radiated power from both antennas is calculated and the ratio taken to arrive at an estimate of the relative efficiency of the antenna under test to that of the reference. This process is described by Equation (1), where η_{test} is the efficiency of the antenna under test, $|E_{standard}|^2$ and $|E_{test}|^2$ are the squared magnitude of the electric field of the standard and test antenna respectively, proportional to the power at that position for the farfield case. *S* denotes the surface over which the electric fields are integrated.

$$\eta_{test} = \frac{\oiint_{Surface} |E_{test}|^2 dS}{\oiint_{Surface} |E_{standard}|^2 dS} \qquad (1)$$

The reference antennas have been externally characterized and have efficiencies of at least 95%. Since we are predominantly interested in trends and coarse predictions here, this is sufficient for our characterization.

The full 3D radiation pattern for the cavity-backed slot antenna for each tuning state and each frequency of interest; 4.5 GHz, 4.8 GHz, 5.3 GHz and 5.8 GHz (as determined by the identified resonances in Figure 6) was measured in a fully anechoic screened chamber employing the set up shown in Figure 7. The laser was mounted on a vertical post, with a slack optical fiber used to direct the light to the desired location whilst allowing free movement of the top rotation mount. An identical set up was used to then measure each of the reference antennas at the desired frequency for subsequent comparison.

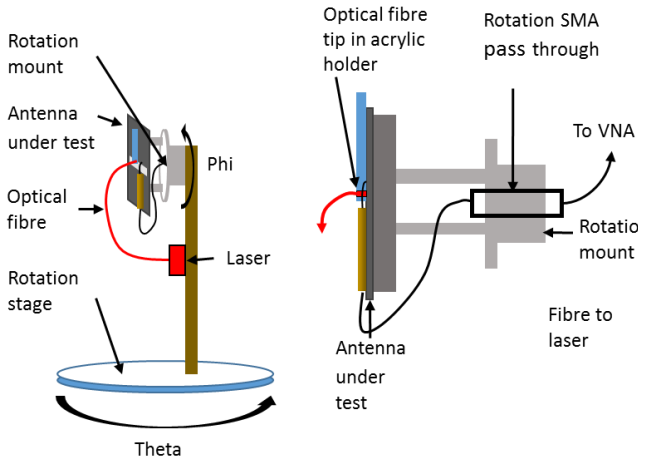

Figure 7 - Schematic showing chamber mounting, Phi and Theta definitions and illumination methodology (left), mounting head detail (right).

The results of this campaign are shown in Figure 8. These generally follow the anticipated behavior predicted by both simulation and the S_{11} measurements. At 4.5 GHz, the antenna is most efficient, and has the highest gain when unilluminated. At 4.8 GHz, there is similar behavior between states where

illumination is applied at either position 1, or position 2. At 5.3 GHz, illumination at Position 2 gives the best performance, and at 5.8 GHz the Position 3 illumination clearly gives the highest efficiency and gain at 62.3 % and 6.9 dBi respectively. There is an additional overall trend that the efficiency of the antenna is generally better at higher frequencies (and in higher tuning states). This may be due to the fact that losses are introduced by the silicon bridging pieces. As illumination is applied to a silicon piece, the losses in the lower numbered pieces (i.e. the pieces away from the feed) are less important as the main radiating fields are concentrated on the feed side of the slot. For example, observing Figure 3, if we illuminate position 3 (effectively creating an electrical short), then the radiating slot no longer encompasses the silicon pieces at positions 1 and 2. Hence only the losses associated with silicon piece 4 are present when illuminating piece 3. This observation would indicate that a future design should seek to reduce the losses caused by these silicon pieces (for example, by reducing further their size and thickness) and using the minimum number required. The bridging piece at position 4 provides no useful tuning state so could be removed, potentially giving an efficiency improvement.

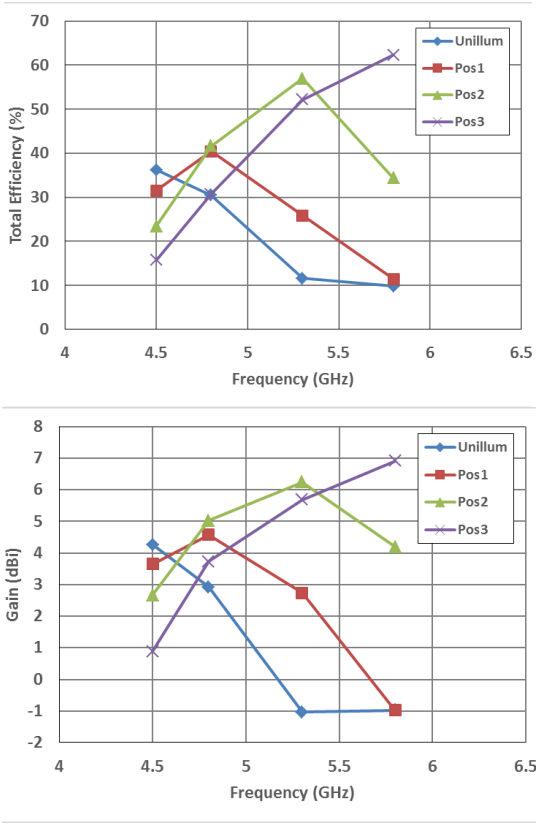

Figure 8 - Measured total efficiency (top) and gain (bottom) of the cavity backed slot antenna at four frequencies for each of the four tuning states.

Summary plots of the measured radiation patterns for all of the tuning states and frequencies of interest are shown in Figure 9. These phi plane (phi = 0°) cuts show the measured S_{21} total power. The values are not normalized, to allow comparison between different frequencies. These plots are consistent with the calculated efficiency values, with the appropriate tuning states giving the highest S_{21} values at each frequency. Additionally, it can be seen that at all frequencies there is a slight squint of the pattern, with all frequencies radiating most strongly close to $\Theta = 20^{o}$, caused mainly by the feed location. There is virtually no back radiation present due to the appropriate ground plane and cavity back used on the antenna. Observing the 5.3 GHz and 5.8 GHz plots, it is interesting to see that with the unilluminated and position 1 illumination states, there is a deep null at $\Theta = 0^{o}$, and strong lobes becoming apparent in the pattern. This indicates that there is some excitation of a higher order mode of the slot. However when the position 3 illumination is applied, the pattern becomes similar to the first order mode behavior seen at 4.5 GHz without illumination. This points towards possible future designs, where illumination can be used to switch between resonant modes of an antenna and alter the radiation pattern whilst maintaining the same resonant frequency.

VI. Conclusion

A tunable slot antenna design has been developed. Through the addition of small silicon bridging pieces and a cavity back to a standard slot antenna, a viable tunable structure has been designed, fabricated and measured. This antenna has a 10 dB tuned range total bandwidth of 32% (from 4.4 GHz to 6.0 GHz) and an RF efficiency of up to 62 %. Pattern reconfigurability has also been seen, with the ability to optically switch a very strong pattern null on and off. Although promising, there remain several challenges to optimizing this design. Firstly, the efficiencies vary significantly between states (with only around 36 % at the lower end of the tuned range). Losses arise from the incorporation of the silicon pieces, and there is scope for further refinement of this aspect of the antenna, as well as a trade-off between efficiency and tunable range (both in terms of bandwidth and in terms of continuity and frequency spacing between switched states). There is significant scope for improving the optical feeding method either through the addition of tailored focusing optics, or the direct incorporation of illumination sources such as surface mount lasers. This work demonstrates that optically induced conductivity in silicon is a viable tuning methodology for antennas, and that good RF efficiencies are achievable.

VII. Acknowledgement

Many thanks to Ken Stevens for assistance and advice in fabricating the antenna and to Andy Murray for help with the photolithography process.

The data in this paper can be found at DOI:xxx

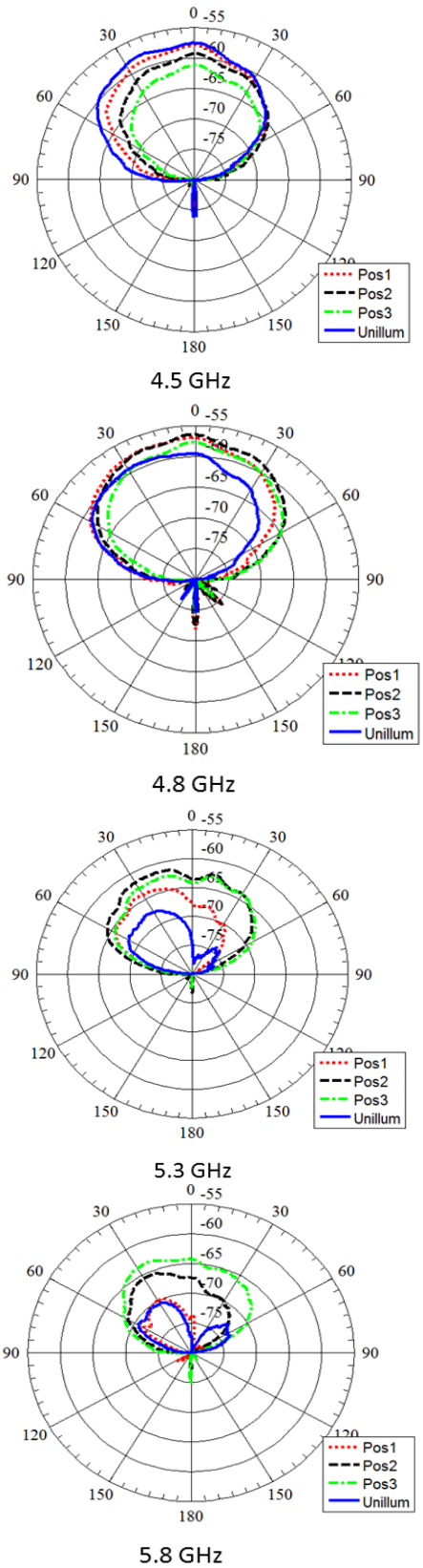

Figure 9 - Measured S_{21} phi plane cut (phi = 0°) of the cavity backed slot antenna. Radius values are in dB, and are un-normalized to allow comparison between frequencies.

REFERENCES

[1] R. Berezdivin, R. Breinig, and R. Topp "Next-Generation Wireless Communications Concepts and Technologies", IEEE Communications Magazine, March 2002, pp108-116

[2] Rappaport, T.S., J.N. Murdock, and F. Gutierrez, State of the Art in 60-GHz Integrated Circuits and Systems for Wireless Communications. Proceedings of the IEEE, 2011. 99(8): p. 1390-1436

[3] Christos G. Christodoulou et al, "Reconfigurable Antennas for Wireless and Space Applications", Proceedings of the IEEE, Vol. 100, No. 7, July 2012

[4] R. L. Haupt and M. Lanagan, "Reconfigurable antennas", IEEE Antennas Propag Magaz 55 (2013), 49–61.

[5] J. Costantine, T. Youssef, S. E. Barbin, and C. G. Christodoulou. "Reconfigurable antennas: Design and applications", Proc. IEEE 103, No. 3 (2015): 424-437.

[6] C.D. Patel, and G. M. Rebeiz, "A high-reliability high-linearity high-power RF MEMS metal-contact switch for DC–40-GHz applications." IEEE Transactions on Microwave Theory and Techniques 60.10 (2012): 3096-3112.

[7] L. L. W. Chow, J. L. Volakis, K. Saitou and K. Kurabayashi, "Lifetime Extension of RF MEMS Direct Contact Switches in Hot Switching Operations by Ball Grid Array Dimple Design", IEEE Electron Device Letters, Vol. 28, No. 6, June 2007, pp479-481

[8] S. Lucyszyn (Ed.), "Advanced RF MEMS", Cambridge University Press, 2010.

[9]Auston, D. H., Cheung, K. P., & Smith, P. R. Picosecond photoconducting Hertzian dipoles. Applied Physics Letters, 45(3), 284, Jan 1984.

[10] Lee, C., Mak, P., & DeFonzo, A. Optical control of millimeter-wave propagation in dielectric waveguides. Quantum Electronics, IEEE, 16(03), 277–288. Jan 1980.

[11] Kowalczuk, E.K., Panagamuwa, C.J., Seager R.D., Vardaxoglou Y.C., Characterising the linearity of an optically controlled photoconductive microwave switch. Loughborough Antennas and Propagation Conference, pp597–600, Nov 2010.

[12] H. Moench et al "High power VCSEL systems and applications" Proc. of SPIE Vol. 9348, 2015 SPIE, doi: 10.1117/12.2076267

[13] A. H. Jeorrett, E. Gu, M. D. Dawson, "Optoelectronic tweezers system for single cell manipulation and fluorescence imaging of live immune cells", Optics Express, Vol. 22, No. 2, 2014, p. 1372-1380

[14] C. J. Panagamuwa, A. Chauraya, and J. C. Vardaxoglou, "Frequency and Beam Reconfigurable Antenna Using Photoconducting Switches" IEEE Transactions on Antennas and Propagation, Vol. 54, No. 2, February 2006

[15] C. D. Gamlath, D. M. Benton and M. J. Cryan, "Microwave Properties of an Inhomogeneous Optically Illuminated Plasma in a Microstrip Gap," in IEEE Transactions on Microwave Theory and Techniques, vol. 63, no. 2, pp. 374-383, Feb. 2015.

[16] M. A. Green "Self-consistent optical parameters of intrinsic silicon at 300 K including temperature coefficients", Solar Energy Materials & Solar Cells 92 (2008) 1305– 1310

[17] Computer Simulation Technology, *CST*. 2016; Available from: https://www.cst.com/

[18] Paul, D.L., et al., "Impact of Body and Clothing on a Wearable Textile Dual Band Antenna at Digital Television and Wireless Communications Bands", IEEE Transactions on Antennas and Propagation, 2013. 61(4): p. 2188-2194